Chemical Thermodynamics and Thermal Analysis 17 (2025) 100160

Contents lists available at ScienceDirect

Chemical Thermodynamics and Thermal Analysis

journal homepage: www.elsevier.com/locate/ctta

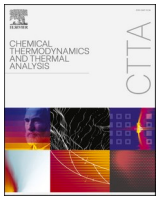

Thermochemical analysis of the behaviour of Cu in Ti nano-strand formation from low-temperature reaction of Al-Fe-Cu powder with CaF_2-SiO_2-Al_2O_3-MgO-MnO-TiO_2 flux

Theresa Coetsee *, Frederik Johannes De Bruin

Department of Materials Science and Metallurgical Engineering, University of Pretoria, Pretoria, 0002, South Africa

ARTICLE INFO

Keywords:
Fluoride
Slag
Gas
Oxy-fluoride
Thermochemistry
Nano

ABSTRACT

The interaction between oxy-fluoride slag and metal in the submerged arc welding process (SAW) includes gas phase reactions. These reactions occur at elevated temperatures in the confined arc cavity, typically between 2000 °C and 2500 °C, making studying the specific chemical interactions challenging. To address this, an experimental method was applied at a lower temperature of 1350 °C to simulate and study the behaviour of the gas species generated from the oxy-fluoride flux, especially when combined with metal powders. In the current study, Al-Fe-Cu metal powders were reacted with CaF_2-SiO_2-Al_2O_3-MgO-MnO-TiO_2 flux to identify the behaviour of copper in the reaction system. Post-reaction three-dimensional slag was analysed using energy dispersive X-ray spectroscopy (EDX) to locate and analyse nano-strands, which confirm gas phase reactions from the oxy-fluoride slag. Thermochemistry calculations explain the observed nano-strand formation from gas-slag-metal reactions. The analyses identified Ti nano-strands with Cu-Fe-Mn-Si fluoride end-caps. Thermochemical analysis indicates that the end-caps formed from oxy-fluoride vaporisation and re-condensation. Ti in the nano-strands originated from TiO_2 in the slag. The following gas-based reaction explains the displacement of Ti by Al from Ti-fluoride gas: $yAl + xTiF_y \leftrightarrow xTi + yAlF_x$. The low-temperature experimental technique can be used to simulate oxy-fluoride slag behaviour in SAW fluxes in terms of gas formation and metal powder assimilation reactions as observed in the SAW process.

1. Introduction

Fluoride-based slags are used in several pyrometallurgical processes such as ESR (electroslag refining), continuous casting of steel and in welding processes such as shielded metal arc welding (SMAW) and submerged arc welding (SAW) [1]. Gas formation from the oxy-fluoride slag in continuous casting mould powders, ESR slags and SAW fluxes is well-documented [2–5]. Mass loss measurements were presented as evidence of fluoride gas formation, and the likely gas species were clarified with thermodynamic analysis [2,3,5]. Increased slag vaporisation was measured with increased TiO_2 content in CaF_2-CaO-Al_2O_3-MgO-Li_2O-TiO_2 ESR slags reacted at 1470 °C to 1530 °C [3]. Decreased vaporisation was measured with increased Al_2O_3 content in the mould flux reacted at 1400 °C. The mould flux contained 14 % CaF_2 and, an initial Al_2O_3 content of 4 % and the maximum Al_2O_3 content at 35 % [4]. Decreasing vaporisation was more pronounced at alumina contents higher than 22 %. Zaitsev et al. [5] analysed the gas evolved from CaF_2-SiO_2-CaO-Al_2O_3-Na_2O-K_2O mould powder heated continuously to 1527 °C. The gas vaporisation sequence measured from the gas analyses identified the initial formation of NaF at 600 °C, KF formation at 883 °C. SiF_4 formation started at 830 °C and increased linearly with increasing temperature. AlF_3 formed from 974 °C to 1200 °C. CaF_2 vaporisation occurred at temperatures higher than 1262 °C. The following gas species were also identified: $NaAlF_4$, Na_2AlF_5, BF_3, and AlOF [5]. The formation of Ti-fluoride gas was confirmed from the interaction of Ti metal and individual fluorides of CaF_2, LiF, and MgF_2 heated to temperatures of 900 °C to 1280 °C in a 10^{-3} Pa vacuum [6]. All these studies confirm that low temperature vaporisation from the oxy-fluoride melt takes place in the form of various gas species in addition to the input fluoride compound, CaF_2. In applying slag-forming welding processes such as submerged arc welding (SAW), fluoride minerals are added to the welding flux to form a shielding gas that protects the weld metal from oxygen, nitrogen, and hydrogen pick-up from the air. In addition, the added CaF_2 forms an oxy-fluoride slag in

* Corresponding author.
E-mail address: theresa.coetsee@up.ac.za (T. Coetsee).

https://doi.org/10.1016/j.ctta.2024.100160
Received 27 September 2024; Received in revised form 29 November 2024; Accepted 28 December 2024
Available online 28 December 2024

Table 1
Chemical composition of flux material.

%MnO	%CaO	%SiO_2	%Al_2O_3	%CaF_2	%MgO	%Fe_2O_3	%TiO_2	%Na_2O	%K_2O
7.0	0.1	20.2	25.7	18.5	22.9	2.7	1.0	1.7	0.2

which the oxides are diluted to limit the release of oxygen in the arc cavity. It is well established that the oxides in the SAW flux decompose in the arc cavity to release oxygen and that this oxygen can quickly oxidise high oxygen affinity metals [7–9].

The temperatures at play in the submerged arc welding (SAW) process vary over a wide range, from 2000 °C to 2500 °C in the arc cavity, down to the weld pool liquidus temperature which is typically close to 1600 °C in carbon steel, and finally to the solidus temperature for weld pool solidification [10,11]. Themochemical modelling of the interaction of gas-slag-metal phases in the SAW process confirmed that fluoride and metal gas species formation at the elevated temperatures in the arc cavity is possible [12]. For example, the following main gas species were identified in the equilibrium calculation for conventional SAW at 2000 °C: CO, Na, NaF, CaF_2, MgF_2, MgF, AlF_3, AlF_2, $NaAlF_4$, TiF_3, $KAlF_4$ as major species, with minor gas species of K, KF, Mg, AlF, Mn, Fe, SiF_4, and SiO present at <1 vol % [12]. In the modified SAW process, aluminium was added as a de-oxidiser element to decrease the partial oxygen pressure in the arc cavity to ensure that the alloying metals remain as metal in the weld pool and as metal vapour in the arc cavity, instead of oxidising to oxides [13,14]. This SAW process modification is especially useful in alloying the weld with high oxygen affinity powdered metals, such as Cr and Ti. The equilibrium calculation for the modified SAW process at 2500 °C with added Al-Ni-Cr-Co-Cu metal powders identified the gas species as Mg, AlF, Fe, Cu, N_2, CO, OAlF, SiO, Mn, Na, MgF, Cr, AlF_2, Al_2O and Al [15]. The gas-slag-metal equilibrium calculations from FactSage thermochemistry software are a good indication of the likely gas phase species expected in the SAW process. The complexity of multi-phase reactions occurring simultaneously in the SAW arc cavity in a brief time frame at high temperatures (2000 °C to 2500 °C) makes the measurement of specific process metallurgy aspects, such as gas formation from the oxy-fluoride slag, difficult. Few real time SAW gas phase analyses were reported and a complicated experimental set-up and specialised equipment are required to analyse the gas phase inside the arc-cavity [16]. Therefore, a low temperature (1350 °C) experimental technique was developed to simulate the oxy-fluoride slag behaviour in SAW fluxes in terms of gas formation and metal powder assimilation reactions as observed in the SAW process [17–19].

Besides the use of gas-slag-metal equilibrium calculations to identify the likely gas phase reactions, the phase chemistry of three dimensional (3D) post-weld slags was measured by scanning electron microscope (SEM) with energy dispersive X-ray spectroscopy (EDX). This work identified oxy-fluoride nano-strand formation within slag cavities [20–22]. It was concluded that the nano-strands observed in the slag cavities formed from re-condensation of arc cavity gasses. Nano-strands were also identified in the low-temperature (1350 °C) reaction of Al-Fe-Ti, Al-Fe-Cr and Al-Fe-Co metal powder mixtures with CaF_2--SiO_2-Al_2O_3-MgO-MnO-TiO_2 flux. However, the nano-strand composition changed depending on the alloying metal powder added, namely Ti or Cr or Co [17–19]. Therefore, nano-strand formation behaviour changes with metal powder addition. This work aims to identify and investigate the nano-strand formation behaviour of Cu in reaction with oxy-fluoride flux in the presence of the added Al and Fe metal powders. Thermochemical analysis and SEM work are used to explain likely reactions that are responsible for nano-strand formation.

2. Material and methods

2.1. Materials

The flux used in this work corresponds to the flux used in previous welding experiments. The chemical composition is summarised in Table 1, with the iron oxide expressed as Fe_2O_3 [12–22]. The mineralogy and chemistry of this flux and its post-weld slag phase chemistry were described elsewhere [23]. The slag phases consist of the liquid oxy-fluoride main phase and spinel crystals ($MgO.Al_2O_3$) [23]. The flux agglomerate particle size was 0.2–1.6 mm.

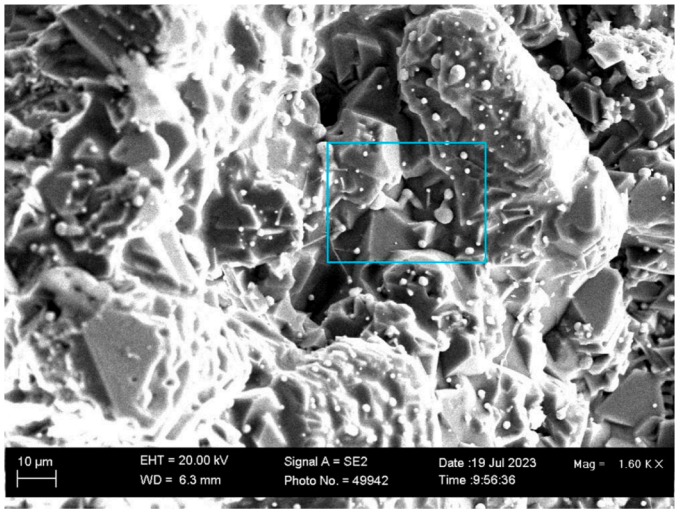

Fig. 1. SEM image of nano-strands at low magnification (x1600).

The added pure metal powders were sourced as follows: Al (99.7 % Al, −1 mm) supplied by Sigma-Aldrich, Cu (99.8 % Cu, −200 µm) supplied by Alfa Aesar, Fe (96.0 % Fe, −50 µm) supplied by Merck. Fe powder was added to simulate the presence of Fe in the SAW of carbon steel, in which iron is sourced from the weld wire and base plate [11–19]. The Al and Cu powders are the same as those applied in the prior SAW work [12–15,20–23].

2.2. Experimental method and analysis

The experimental methods used in the preparation and reaction of the sample mixture are the same as those reported previously [17–19]. Sample preparation consisted of weighing and mixing the solid reactants of flux and metal powders. Each metal powder of Al, Fe and Cu was added at eight mass% of the overall mixture. A cylindrical pellet was formed by applying a 10 ton load to the sample mixture of 19.5 gram contained in a 20 mm diameter mould. The sample mixture was compressed into a pellet of 30 mm height.

Before loading the pellet into the furnace, the pellet was placed onto the pellet holder. The pellet holder consisted of a low carbon steel plate of dimensions of 65 mm square and 2 mm thickness. The pellet holder had a pressed circular recessed centre to assist in pellet placement. A muffle furnace was pre-heated to 1350 °C and soaked for 12 h at 1350 °C. Following this soaking time, the pellet holder and pellet were placed into the muffle furnace and reacted for 6 min in an air atmosphere. The use of air as an unmodified gas atmosphere accords with SAW gas phase conditions of using the flux to generate the shielding gas without the addition of any other gasses. Upon completion of the reaction time, the pellet was removed from the furnace to cool down in the air. The cooled pellet was sectioned through its middle, and the inner faces were coated with gold. The three-dimensional (3D) sample was analysed by scanning electron microscope (SEM). A Zeiss crossbeam 540 FEG (field emission

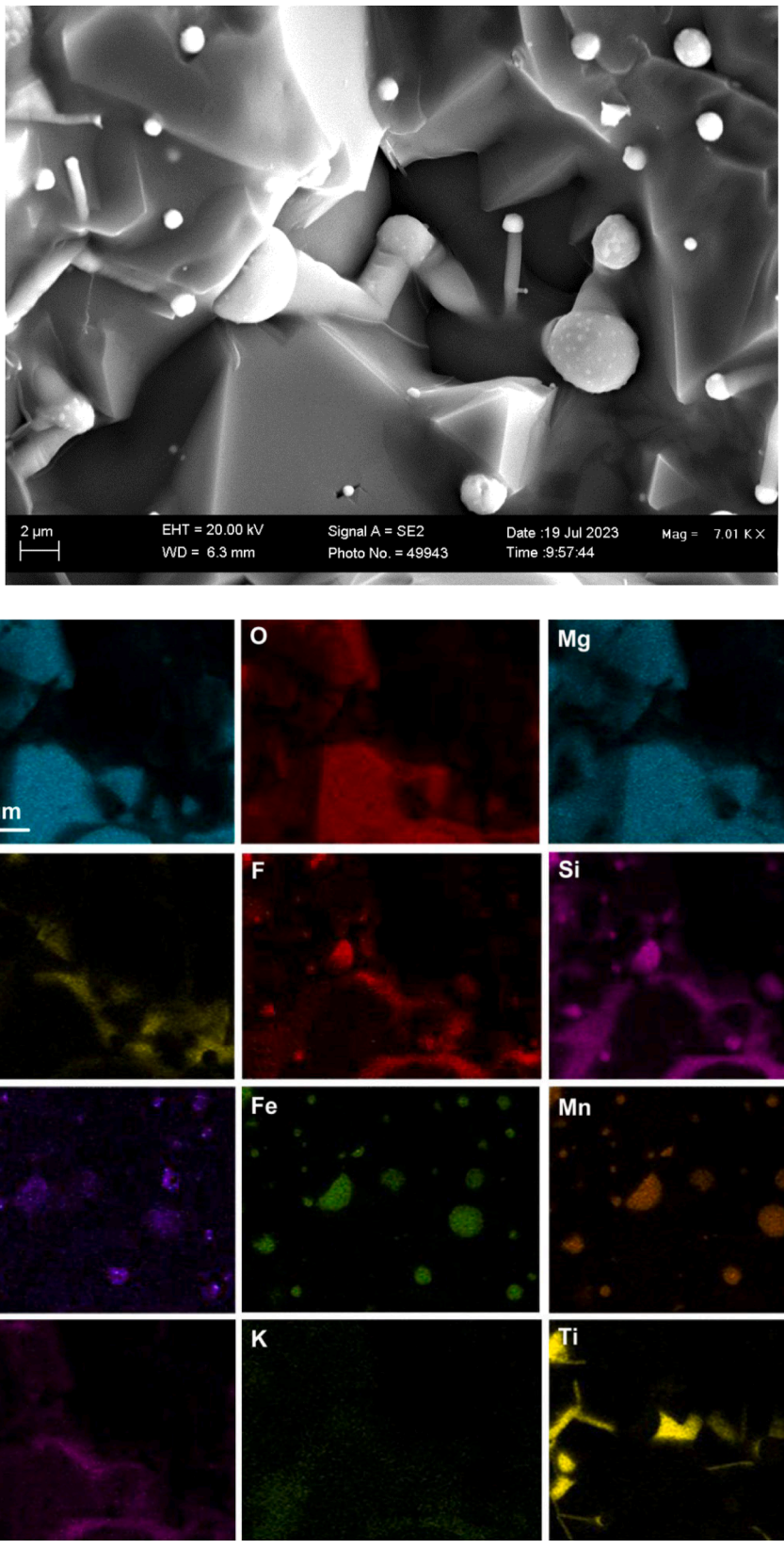

Fig. 2. (a): SEM image (x7010) of analysed area as marked in Fig. 1; (b): EDX map of area in Fig. 2(a).

gun) SEM with energy dispersive X-ray spectroscopy (EDX) probe operated at 20 kV was used to perform phase chemical analyses of the 3D sample.

3. Results

Fig. 1 at low magnification (x1600) displays the phenomena of nano-strands typically observed in the cavities of the reacted flux-alloy

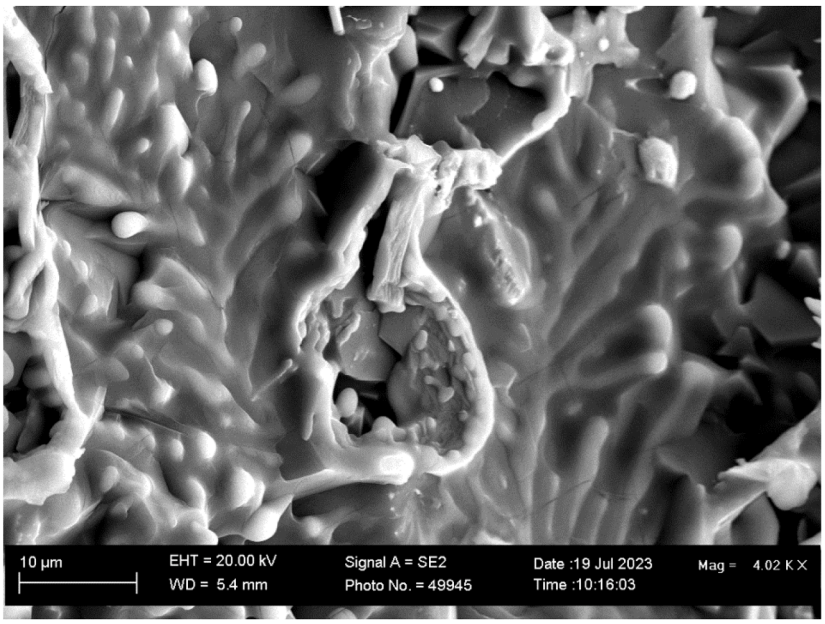

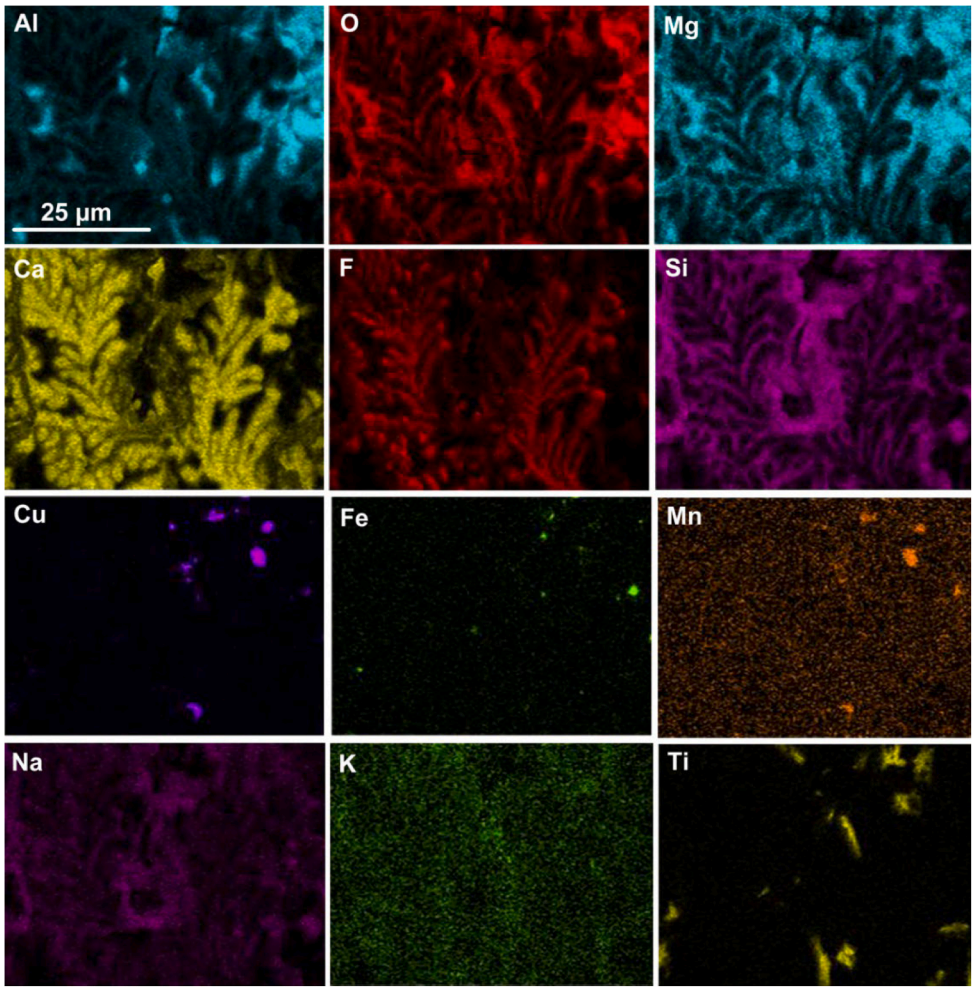

Fig. 3. (a): SEM image (x4020) of leaf structured CaF_2; (b): EDX map of area in Fig. 3(a).

mixture. The blocked area in Fig. 1 is shown as the field of view (FOV) in Fig. 2(a) at higher magnification (x7010). This image clearly shows the nano-strand morphology, and Fig. 2(b) shows the nano-strand chemistry in the form of EDX element maps. The Cu EDX map brightness was increased since the contrast between purple and black is weak. The presence of copper-containing oxy-fluoride nano-strands can be used to confirm that gas phase reactions occurred in nano-strand formation. The reasoning is that the copper was added as large metallic copper powder

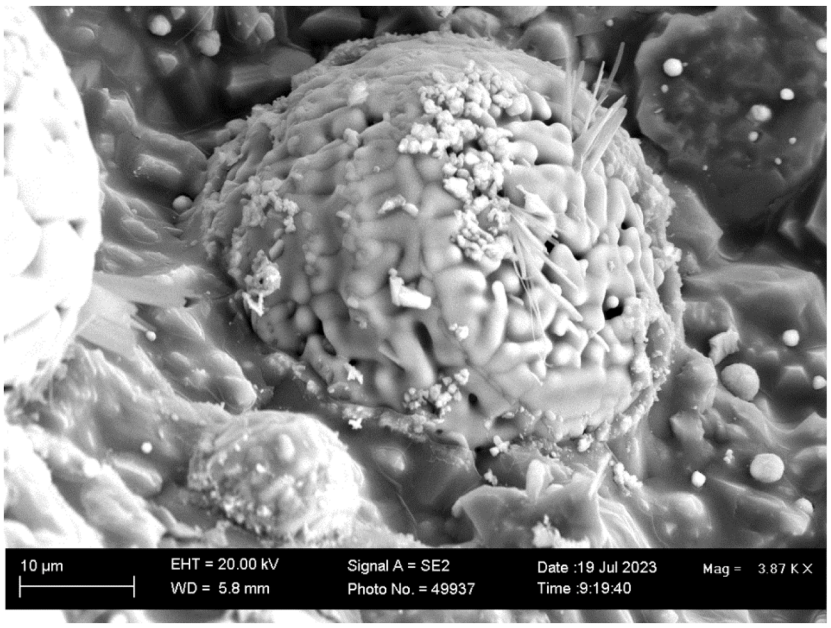

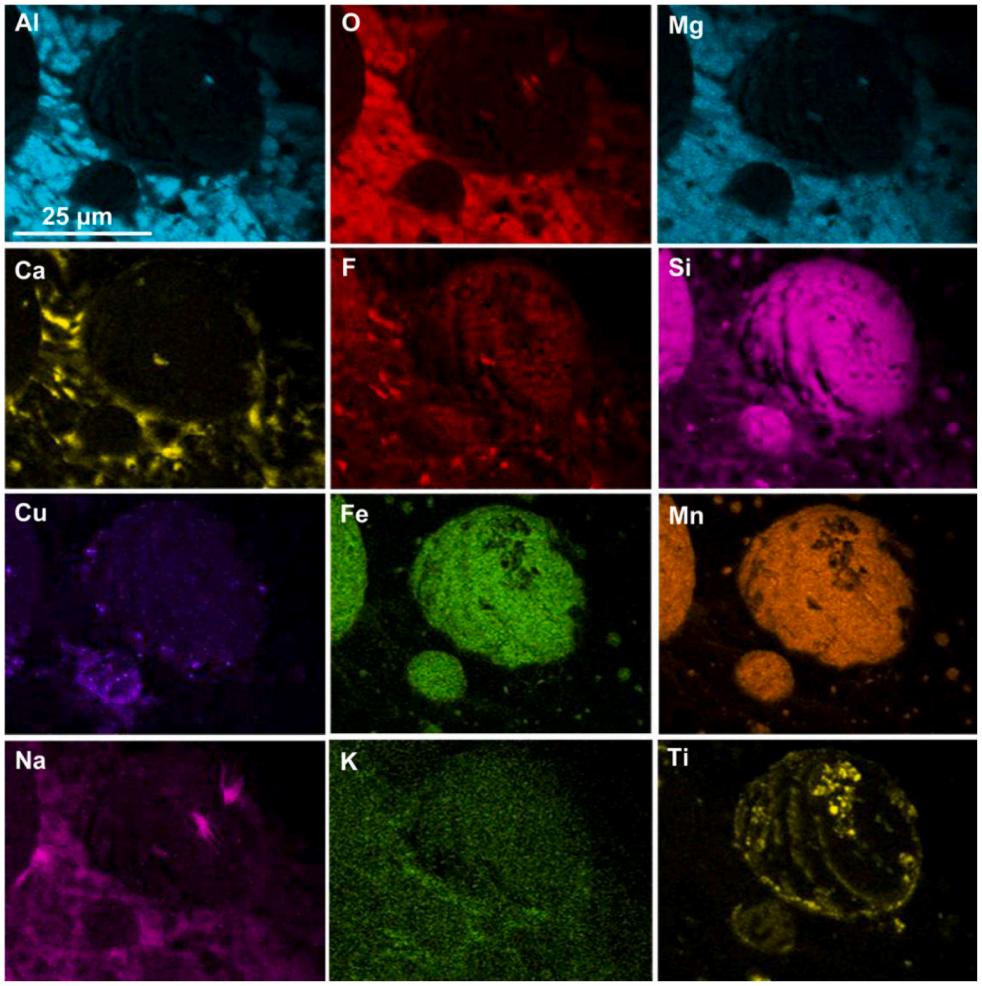

Fig. 4. (a): SEM image (x3870) of sphere structures; (b): EDX map of area in Fig. 4(a).

particles of −200 µm. Thus, the copper could only be incorporated at nano-scale, at different sites from the copper metal particles, with the assistance of gas phase reactions. This interpretation was also applied in the reaction of Al-Fe-Ti, Al-Fe-Cr and Al-Fe-Co metal powders with the same CaF_2-SiO_2-Al_2O_3-MgO-MnO-TiO_2 flux used in this work [17–19]. It is seen in Fig. 2(b) that copper is contained in the nano-strand end-caps as Cu-Fe-Mn-Si fluoride. In contrast, the nano-strands contain pure Ti, similar to the nano-strands previously observed in Al-Fe-Co reaction

Table 2
Average EDX analysis of the field of view in Figs. 2–5.

Figure	%O	%F	%Na	%Mg	%Al	%Si	%K	%Ca	%Ti	%Cu	%Mn	%Fe
2	38.2	4.3	1.1	13.0	21.0	5.0	0.3	3.3	5.5	0.6	4.0	3.3
3	29.6	23.4	2.0	8.0	8.1	5.6	0.3	20.5	1.2	0.7	0.3	0.2
4	27.7	4.3	2.0	8.9	12.3	14.4	0.2	2.8	2.6	1.6	17.7	4.0
5	6.6	1.2	0.6	4.8	4.4	2.0	0.0	1.5	0.3	72.1	3.9	2.5
Maximum σ	0.14	0.12	0.06	0.05	0.07	0.03	0.01	0.06	0.03	0.22	0.04	0.03
Glass [23]	34.3	12.3	2.0	12.4	6.8	12.1	0.3	12.8	0.6	0.0	5.7	0.7
Glass [23]	34.1	12.7	2.0	12.3	6.2	12.4	0.0	13.3	0.7	0.0	5.8	0.5
Flux	35.3	8.7	0.6	13.4	13.2	9.2	0.2	9.3	0.6	0.0	5.3	4.2

with oxy-fluoride flux [19]. Interestingly, two end-caps appear in the large nano-strand in the centre of Fig. 2. Therefore, the Ti nano-strand growth seems to be multi-phased to form alternating chemistries of pure Ti and Cu-Fe-Mn-Si fluoride end-caps. This behaviour fits better with re-condensation from the gas phase than diffusion from the slag phase. The slag consists of spinel crystals, seen as angular Al-Mg-O areas in the EDX maps, embedded in Ca-F-Si-Na-K glass phase. In addition to the formation of nano-strands, the formation of different slag morphologies is displayed at lower magnification in Figs. 3 and 4.

Fig. 3 at (x4020) shows leaf-shaped phase areas of Ca-F embedded and covered by the Al-O-Mg-Si-Na glass phase. Metallic Mn and Cu appear on the surface of the glass phase as two alloy spots in the top right-hand corner of Fig. 3, and Mn-Cu-Fe alloy spots in a few places. The size of the Mn-Cu alloy sports is close to 3 μm in size, indicating gas phase transport. The distribution of Ti is not homogenous and its association in Fig. 3 is unclear. Fig. 4 shows the sphere morphology often seen in cavities inside the 3D post-weld slag samples consisting of multi-element oxy-fluoride, including Cu [15,21–22]. The spheres are typically embedded in the matrix phase containing glass and spinel. The chemical association in the spheres in Fig. 4 appears similar to that of the nano-strands in Fig. 2 in terms of F-Si-Fe-Mn-Cu-Ti-Na, even though the Cu and Ti appear as spots and strings and the F-Si-Fe-Mn appear as the main constituents in the sphere surface. The absence of oxygen in the nano-structures in Fig. 2 and the spheres in Fig. 4 may indicate that less oxygen-containing gasses were formed or were incorporated at 1350 °C than at the high temperatures in the SAW cavity.

The presence of Na-O-containing blades protruding from the sphere surface is in accordance with previous observations of similar structures in post-weld slags [15]. Consideration of the sphere dimensions in Fig. 4, compared to the added metal powder sizes of the Fe and Cu, −50 μm and −200 μm respectively, indicates gas phase reaction involvement in forming the Cu-containing spheres of F-Si-Fe-Mn-Cu-Ti-Na chemistry. The average analyses of the FOV in each Figure are summarised in Table 2. The maximum standard deviation values (σ) shown in Table 2 indicate the SEM-EDX analysis quality. The flux analysis from Table 1 is shown in the last line of Table 2. Similarly, the glass phase SEM-EDX analyses in post-weld slag from welding without metal powder additions are also shown in the second and third last lines of Table 2 [23]. The FOV analyses of Figs. 2–4 appear different to the flux analyses and glass phase analysis values, especially concerning Cu and Ti content. The composition differences indicate that the 3D feature did not simply evolve from the underlying flux of glass phases.

The limited incorporation of Cu into the nano-strands may be explained by the bulk alloy formation of the low melting point copper-based alloy, as displayed in Fig. 5. Table 2 shows the alloy analysis. The presence of significant quantities of Al, Mg, Si, Ca, Mn, Fe, O, and F in the Cu alloy indicates gas phase reaction transfer from the molten flux to the bulk alloy surface.

4. Discussion

The following section shows the probable gas species formation from thermochemistry calculations in the form of Gibbs free energy values. Thermochemical software FactSage 7.3 was used for the calculations [24]. The Reaction module was used to calculate the reaction Gibbs free energy values using FactPS and FToxid databases. Calculations were made for 1300–2000 °C to compare the relative thermodynamic favourability of the reactions at 1350 °C, the reaction temperature applied in this work, to that at much higher temperatures encountered in SAW. The liquid phase process temperatures in the SAW process vary from elevated temperatures in the order of 2000–2500 °C in the arc cavity to the weld pool liquidus temperature, in the order of 1600 °C for carbon steel [2,3].

As a first consideration, as in our previous work on SAW, we considered the vapour pressure of the pure metals, as displayed in Fig. 6 [20,21]. It is seen that K, Na and Mg have high vapour pressures, even at 1300 °C. The vapour pressures of Mn, Al, Cu, Fe, Si and Ti are lower but not insignificant. The Al added to the SAW reaction system ensures a low partial oxygen pressure in the SAW process to prevent oxidation of high oxygen affinity elements such as Ti and Cr [13,14]. Similarly, at a lower temperature of 1350 °C, as applied in the current simulation experiments, the added Al metal powder lowers the partial oxygen pressure in the reaction mass [17–19].

The thermodynamic favourability of the reaction of metals with F_2 gas, as displayed in reaction (1), was considered a first reaction analysis step. The phrase "(most stable)" in reaction (1) refers to the selection made in the Reaction module in FactSage to change the phase state with temperature. However, the presence of F_2 gas at low temperatures is unlikely because the fluoride compound in the flux is CaF_2, and CaF_2 gas is the favoured species, not F_2 [24]. However, to illustrate the relative stability of individual metal fluoride species, the calculation of the Gibbs free energy of reaction (1) is required, as displayed in Fig. 7.

$$M(\text{most stable}) + (x/2)F_2(g) \leftrightarrow MF_x(\text{most stable}) \quad (1)$$

The fluorides are present as liquid or gas in the 1300–2000 °C temperature range. CuF_2, KF, NaF, FeF_2, and MnF_2 transition from liquid to gas as indicated by filled circle icons in Fig. 7 and summarised in Table 3. The following fluorides are in the gaseous state at 1350 °C: SiF_4, AlF_3, AlF_2, AlF, TiF_4, TiF_3, TiF_2, TiF, FeF_3.

The relative position of the lines in Fig. 7 indicates the most favoured metal reactant that can displace the metal from a metal fluoride. For example, if Al metal reacts with any of the metal fluorides positioned above the AlF_3 line in Fig. 7, for example, the FeF_3 line, then AlF_3 will be formed by displacing Fe from its fluoride via reaction (2).

$$Al(g) + FeF_3(g) \leftrightarrow Fe(g) + AlF_3(g) \quad (2)$$

Although metallic Al is absent in the flux, it was added as metal powder. Typically, the Gibbs free energy values for the reaction of a metal with $F_2(g)$ are more negative in value than that of the reaction of the metal with $O_2(g)$ [18]. This indicates that added metals will react to form fluorides instead of forming oxides.

Although reaction (2) indicates AlF_3 formation, alternate Al-fluoride gas species of AlF_2 and AlF can also form, as expressed in the general chemical reaction expression in reaction (3), M = metal. This effect is displayed in Figs. 8(a), (b), (c), indicating that Al can displace the metals from most of the fluorides to form $AlF(g)$, $AlF_2(g)$ and $AlF_3(g)$, and Cu is most easily displaced from CuF_2. Therefore, the formation of Ti nano-

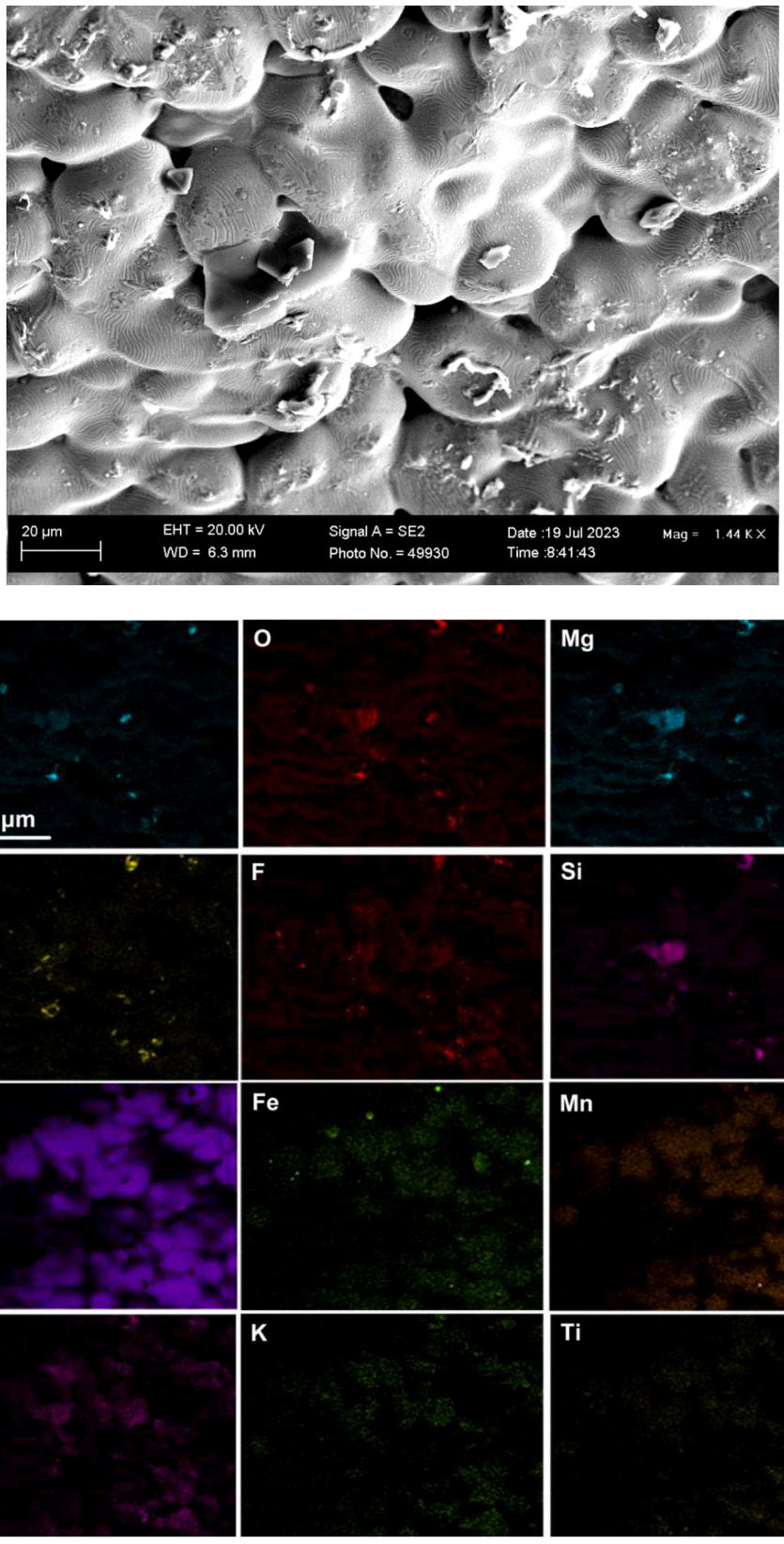

Fig. 5. (a): SEM image (x1440) of copper alloy; (b): EDX map of area in Fig. 5(a).

strands is thermodynamically possible via reaction (3) in which Al displaces Ti from TiF_4, TiF_3 and TiF via gas phase reactions to form Ti nano-strands via the re-condensation of Ti vapour. The subsequent re-condensation of metals displaced by Al from their fluorides and some of the unreacted fluorides can account for the Fe-Mn-Si-Cu fluoride spherical end-caps at the end of the nano-strands, as displayed in Fig. 2. The formation of pure Ti nano-strands with metal-fluoride end-caps appears similar to the observations in the reaction of Al-Fe-Co metal

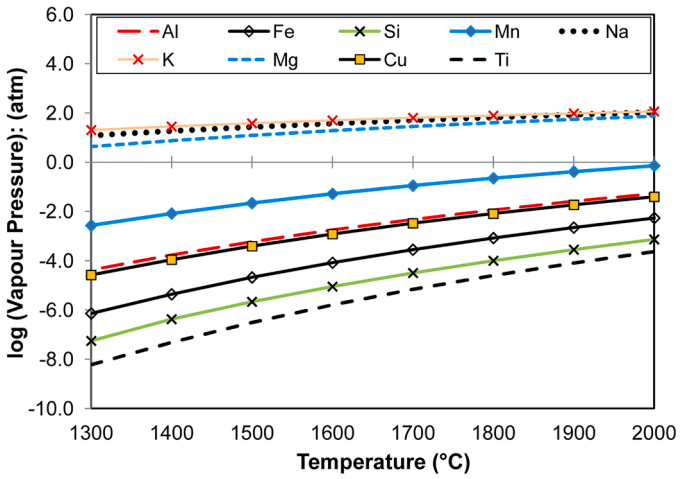

Fig. 6. Vapour pressure of metals (calculated in FactSage 7.3).

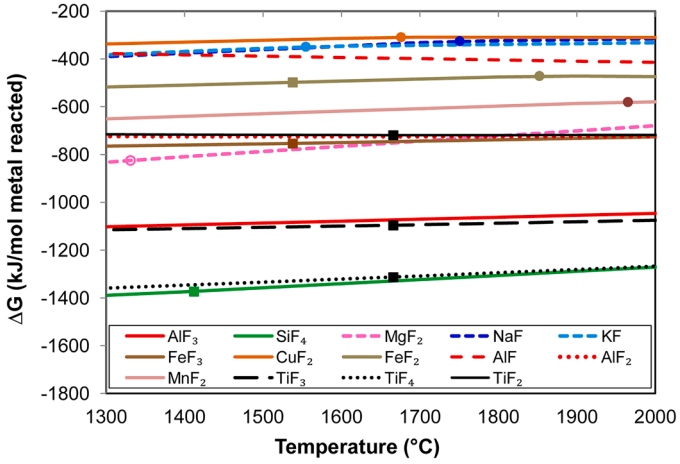

Fig. 7. Gibbs free energy of metal-fluoride formation via reaction (1): open circle = $MF_X(s) \rightarrow MF_X(l)$; filled circle = $MF_X(l) \rightarrow MF_X(g)$; filled square = M(s)→M(l); dashed line = M(g).

Table 3
Metal fluoride phase transitions in the temperatures range of 1000 °C to 2600 °C (FactSage 7.3 data): (g) = gas; (l) = liquid; (s) = solid.

Fluoride	Gas Phase	(s)→(l)	(s)→(g)	(l)→(g)
SiF_4	(g)			
CaF_2		1419		2531
AlF_3		1291		
AlF_2	(g)			
AlF	(g)			
CuF_2		836		1673
TiF_4	(g)			
TiF_3			1035	
TiF_2			1103	
TiF	(g)			
MnF_2				1965
FeF_2				1852
FeF_3	(g)			
MgF_2		1331		2263
KF				1554
NaF				1750

powder mixtures with the same CaF_2-SiO_2-Al_2O_3-MgO-MnO-TiO_2 flux [19]. In the latter case, the end-caps consisted of Co-Mn-Fe fluoride. These gas-based reactions that formed the Ti nano-strands and

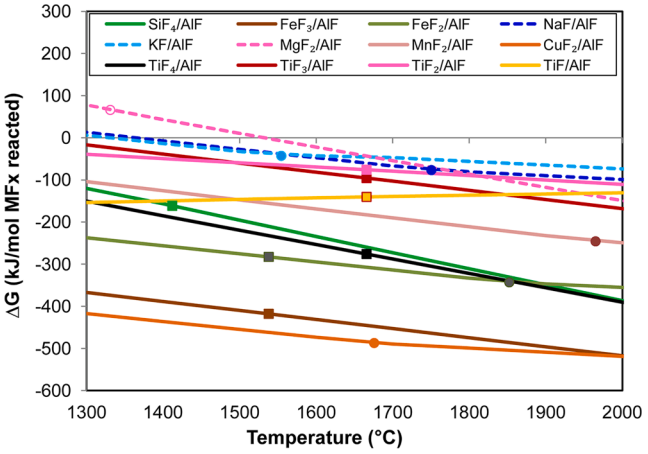

Fig. 8a. Gibbs free energy of element displacement via reaction (3) with AlF(g) formation: open circle = $MF_X(s) \rightarrow MF_X(l)$; filled circle = $MF_X(l) \rightarrow MF_X$ (g); filled square = M(s)→M(l); dashed line = M(g).

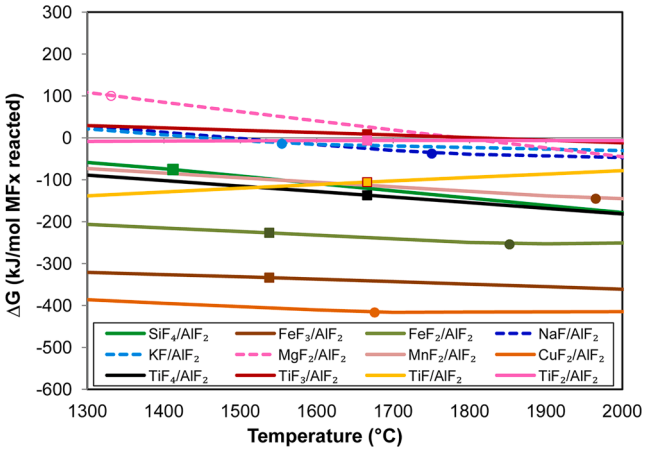

Fig. 8b. Gibbs free energy of element displacement via reaction (3) with AlF_2(g) formation: open circle = $MF_X(s) \rightarrow MF_X(l)$; filled circle = $MF_X(l) \rightarrow MF_X(g)$; filled square = M(s)→M(l); dashed line = M(g).

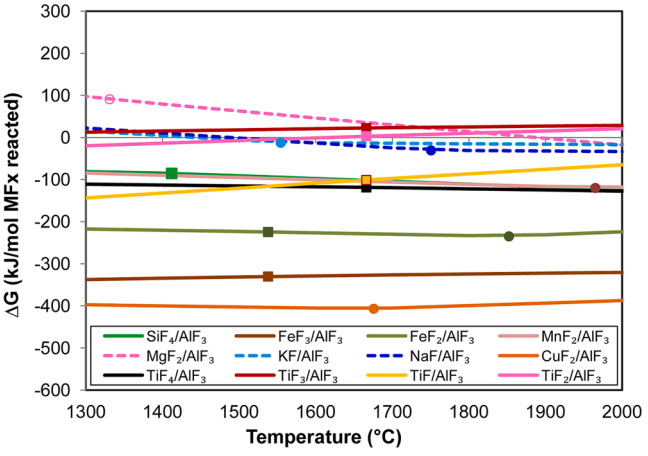

Fig. 8c. Gibbs free energy of element displacement via reaction (3) with AlF_3(g) formation: open circle = $MF_X(s) \rightarrow MF_X(l)$; filled circle = $MF_X(l) \rightarrow MF_X(g)$; filled square = M(s)→M(l); dashed line=M(g).

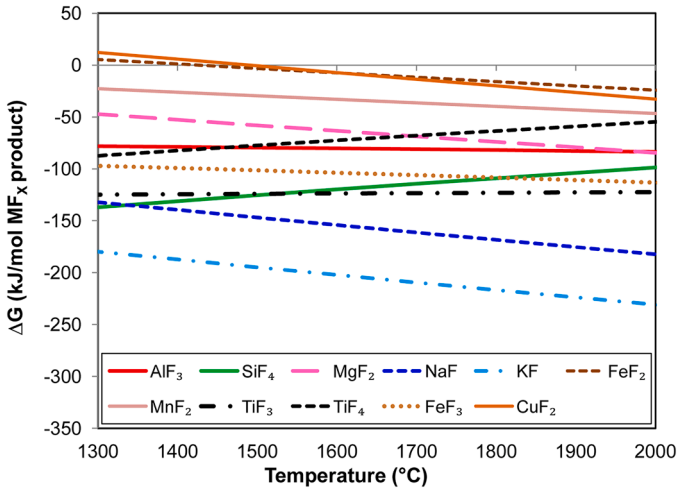

Fig. 9. Gibbs free energy of fluoride formation via reaction (4).

Fe-Mn-Si-Cu fluoride end-caps in Fig. 2 can also explain the formation of spheres seen in Fig. 4 since the same elements are present in both instances.

$$yAl + xMF_y \leftrightarrow xM + yAlF_x \quad (3)$$

The following section explains the likely reactions of metal fluoride formation from the only added fluoride, CaF_2. The fluoride compounds in the liquid state are not individual phases because CaF_2 and the oxides combine chemically into a liquid oxy-fluoride glass phase. Similarly, the formation reactions of fluorides differ from reaction (1) because the formation of large quantities of $F_2(g)$ is unlikely at low temperatures [24]. The formation of fluoride gas other than CaF_2 is possible as vaporisation from the oxy-fluoride glass phase. However, SAW flux research often presents the following reaction as a pathway to convert CaF_2 gas to other fluoride gasses [7,25].

$$SiO_2(slag) + 2CaF_2(g) \leftrightarrow 2CaO(slag) + SiF_4(g) \quad (4)$$

Fig. 9 shows the Gibbs free energy for reactions similar to reaction (4) to form each metal fluoride gas product (MF_X) with inputs of 1 atm CaF_2 partial pressure; the product fluoride gas at 0.10 atm partial pressure; the activity of the liquid flux oxide in the oxy-fluoride slag was set to 0.5 and the activity of CaO set to 0.01 (a_{CaO}=0.01). The activity and partial pressure values are based on value selections made for SAW [23]. It is seen that KF is most easily formed. The lines for NaF formation cross the line for SiF_4 formation at 1342 °C. Therefore, at 1350 °C, the formation of NaF is favoured ahead of SiF_4 formation via reaction (4). The next most probable reaction with CaF_2 at 1350 °C is the formation of TiF_3, FeF_3, TiF_4, AlF_3, MgF_2, and MnF_2. Formation of FeF_2 and CuF_2 at low temperatures appears less likely. However, different chemical conditions of gas partial pressure and activity values may shift the lines for FeF_2 and CuF_2 negative since the Gibbs free energy lines are close to zero in Fig. 9.

The thermochemical analysis explains the likely gas-phase reaction formation sequence of nano-strand and end-cap formation in the reaction system. However, in considering the possibility of Ti nano-strand formation from the oxy-fluoride slag rather than from the gas phase, the following can be noted: the diffusion of low concentration Ti in the slag (1 % TiO_2 in Table 1) is too slow to account for the observed Ti nano-strand formation at various positions in the sample. If Ti diffusion in the slag was fast, the Ti nano-strands would have been re-absorbed at its formation site and dissipated evenly into the slag area surrounding the nano-strand base. It is seen that the Ti nano-strands appear as distinct strands with no Ti contained in the slag at the base of the Ti-strand. Previous studies showed that low-temperature metal vapour deposition from the decomposition of metal halides under reducing gas conditions of a hydrogen atmosphere is possible and that distinct metal whiskers formed [26,27]. Cu, Ni, Fe and Co metal whiskers were formed upon re-condensation of respective Br, Cl, or I halides at temperatures below 900 °C. Whiskers could not be formed from fluorides under the same temperature and hydrogen gas conditions due to fluoride stability [26].

The formation of MgO whiskers from the re-condensation of Mg vapour and O_2 gas is well documented [28–30]. MgO dissociation is possible under controlled conditions of a reducing atmosphere, typically with the addition of carbon as reductant, to from MgO whiskers in-situ via VLS (vapour-liquid-solid) and VS (vapor-solid) processes [28–30]. The observation of spherical nanoparticles at the end of whiskers/nano-strands was reported [28,30]. Spherical nanoparticles were reported to consist of MgO, the same as chemistry as in the supporting whiskers [28]. In some instances the spherical nanoparticles contain metals when these were added as catalysts or elements from the oxide slag such as Ca, Al and Si when the slag was the catalyst element source [28,30].

In comparison, the nano-strands in this work consist of pure Ti with Cu-Fe-Mn-Si fluoride end-caps. The absence of oxygen from the nano-strands is notable and indicates that oxygen has been captured by the added Al reductant chemical. The presence of fluoride in the Cu-Fe-Mn-Si containing end-caps as displayed in Fig. 2(a) points to fluoride gas formation and re-condensation, and not pure metal catalysis as reported in MgO whisker/nano-strand formation.

In conclusion, it is seen that the low-temperature technique applied in this work to react Al-Fe-Cu metal powders and CaF_2-SiO_2-Al_2O_3-MgO-MnO-TiO_2 flux can simulate the vaporisation and re-condensation behaviour of copper in the SAW process. The extent of reaction may be improved with increased reaction time, and the formation of low-melting point copper-based alloy should be better controlled.

5. Conclusions

Low-temperature (1350 °C) reaction of oxy-fluoride flux with metal powders can be used to simulate the gas-phase reactions in SAW. The formation of copper-containing nano-strand end-caps as Cu-Fe-Mn-Si confirms that copper was transferred via gas phase reactions from the larger copper powder particles of −200 μm. The formation of pure Ti nano-strands is explained by a thermochemical analysis of the reaction system, which confirms the metal displacement from metal fluorides by added Al powder.

Data availability

Data will be made available on request.

CRediT authorship contribution statement

Theresa Coetsee: Writing – review & editing, Writing – original draft, Visualization, Methodology, Investigation, Formal analysis, Data curation, Conceptualization. **Frederik Johannes De Bruin:** Writing – review & editing, Writing – original draft, Visualization, Methodology, Investigation, Formal analysis, Data curation, Conceptualization.

Declaration of competing interest

The authors declare that they have no known competing financial interests or personal relationships that could have appeared to influence the work reported in this paper.

Acknowledgements

The University of Pretoria supported this work. The authors thank Erna van Wilpe and Coenraad Snyman, colleagues at the Laboratory for Microscopy and Microanalysis (University of Pretoria), for their advice

and assistance on SEM imaging and analysis.

Data availability

Data will be made available on request.

References

[1] G.E. Linnert, Welding Metallurgy-Carbon and Alloy Steels, Volume I-Fundamentals, 4th ed., American Welding Society (AWS), Miami, FL, USA, 1994, pp. 706–758.
[2] T. Schultz, B. Lychatz, N. Haustein, D. Janke, Structurally based assessment of the influence of fluorides on the characteristics of continuous casting powder slags, Metall. Trans. B 44 (2013) 317–326.
[3] J. Ju, G. Ji, J. An, C Tang, Effect of TiO_2 on fluoride evaporation from CaF_2-$CaOAl_2O_3$-MgO-Li_2O-(TiO_2) slag, Ironmaking Steelmaking 48 (2020) 109–115.
[4] J. Gao, G. Wen, Q. Liu, W. Tan, P. Tang, Effect of Al_2O_3 on the fluoride volatilization during melting and ion release in water of mould flux, J. Non-Cryst. Solids 409 (2015) 8–13.
[5] A.I. Zaitsev, A.V. Leites, A.D. Litvina, B.M. Mogutnov, Investigation of the mould powder volatiles during continuous casting, Steel Res 65 (1994) 368–374.
[6] V.P. Krasovskyy, Interaction of single-crystalline metal fluorides with titanium-containing melts, Powder Metall. Met. Ceram. 58 (2019) 334–340.
[7] C.S. Chai, T.W. Eagar, Slag metal reactions in binary CaF_2-metal oxide welding fluxes, Weld. J. 61 (1982) 229S–232S.
[8] A. Polar, J.E. Indacochea, M. Blander, Electrochemically generated oxygen contamination in Submerged Arc Welding, Weld. J. 69 (1990) 68S–74S.
[9] T. Lau, G.C. Weatherly, A Mc Lean, The sources of oxygen and nitrogen contamination in Submerged Arc Welding using CaO-Al_2O_3 based fluxes, Weld. J. 69 (1985) 343S–347S.
[10] C.S. Chai, T.W. Eagar, Slag-metal equilibrium during Submerged Arc Welding, Metall. Trans. B 12 (1981) 539–547.
[11] U. Mitra, T.W. Eagar, Slag-metal reactions during welding: part 1. Evaluation and reassessment of existing theories, Metall. Trans. B 22 (1991) 65–71.
[12] T. Coetsee, R.J. Mostert, P.G.H. Pistorius, P.C. Pistorius, The effect of flux chemistry on element transfer in Submerged Arc Welding: application of thermochemical modelling, Mater. Res. Technol. 11 (2021) 2021–2036.
[13] T. Coetsee, F.J. De Bruin, Reactions at the molten flux-weld pool interface in submerged arc welding, High Temp. Mater. Processes 40 (2021) 421–427.
[14] T. Coetsee, F.J. De Bruin, Improved titanium transfer in Submerged Arc Welding of carbon steel through aluminium addition, Miner. Process Extr. Metall. Rev. 43 (2021) 771–774.
[15] T. Coetsee, F.J. De Bruin, EERZ (Effective Equilibrium Reaction Zone) Model of Gas-Slag-Metal Reactions in the Application of Unconstrained Al-Ni-Cr-Co-Cu Metal Powders in Submerged Arc Welding: model and 3D Slag SEM Evidence, Processes 11 (2023) 2110.
[16] G. Gött, A. Gericke, K.-M. Henkel, D. Uhrlandt, Optical and spectroscopic study of a submerged arc welding cavern, Weld. J. 95 (2016) 491–499.
[17] T. Coetsee, F.J. De Bruin, Nano-strand formation in CaF_2-SiO_2-Al_2O_3-MgO flux reacted at 1350 °C with Al-Ti-Fe powder: SEM analyses and gas reaction thermochemistry, J. Solid State Chem. 331 (2024) 124547.
[18] T. Coetsee, F.J. De Bruin, Low temperature vaporisation of Cr from fluoride flux reacted at 1350 °C with Al–Cr–Fe powder: thermochemical analysis of gas phase reactions and nano-strand formation, J. Mater. Res. Technol. 30 (2024) 1159–1171.
[19] T. Coetsee, F De Bruin, Nano-Strand Formation via Gas Phase Reactions from Al-Co-Fe Reacted with CaF_2-SiO_2-Al_2O_3-MgO Flux at 1350 °C: SEM Study and Thermochemistry Calculations, Processes 12 (2024) 1342.
[20] T. Coetsee, F.J. De Bruin, Insight into the Chemical Behaviour of Chromium in CaF_2-SiO_2-Al_2O_3-MgO Flux Applied in Aluminium-Assisted Alloying of Carbon Steel in Submerged Arc Welding, Minerals 12 (2022) 1397.
[21] T. Coetsee, F.J. De Bruin, Chemical Behaviour of Copper in the Application of Unconstrained Cr-Ni-Al-Cu Metal Powders in Submerged Arc Welding: gas Phase Thermodynamics and 3D Slag SEM Evidence, Processes 11 (2023) 351.
[22] T. Coetsee, F. De Bruin, Gas Formation of Cobalt and Copper in the Application of Unconstrained Co-Cr-Al-Cu Metal Powders in Submerged Arc Welding: gas Phase Thermodynamics and 3D Slag SEM Evidence, Processes 11 (2023) 1116.
[23] T. Coetsee, Phase chemistry of Submerged Arc Welding (SAW) fluoride based slags, Mater. Res. Technol. 9 (2020) 9766–9776.
[24] C.W. Bale, E. Bélisle, P. Chartrand, S. Decterov, G. Eriksson, A.E. Gheribi, K. Hack, I.-H. Jung, Y.-B. Kang, J. Melançon, et al., Reprint of: factSage thermochemical software and databases, 2010–2016, CALPHAD. 55 (2016) 1–19.
[25] T. Lau, G.C. Weatherly, A Mc Lean, Gas/Metal/Slag reactions in Submerged Arc Welding using CaO-Al_2O_3 based fluxes, Weld. J. 70 (1986) 31S–38S.
[26] S.S. Brenner, The growth of whiskers by the reduction of metal salts, Acta Metall 4 (1956) 62–74.
[27] S.S. Brenner, G.W. Sears, Mechanism of whisker growth-III Nature of growth sites, Acta Metall 4 (1956) 268–270.
[28] A. Yamaguchi, S. Hashimoto, Growth if magnesia whiskers, Ceram. Int. 18 (1992) 301–305.
[29] M. Zhao, X.L. Chen, W.J. Wang, Y.J. Ma, Y.P. Xu, H.Z. Zhao, Self-catalyzed growth if magnesium oxide nanorods, Mater. Lett. 60 (2006) 2017–2019.
[30] D. Kumar, P.C. Pistorius, Use of slag (CaO-Al_2O_3-SiO_2-MgO) droplet as a catalyst to grow MgO whiskers through VLS machanism, Ceram. Int. 43 (2017) 15478–15485.